

Regular article

An Easy-to-use Genotoxicity Assay Using EGFP-MDC1-expressing Human Cells

Shun Matsuda¹, Ryo Matsuda², Yoko Matsuda¹, Shin-ya Yanagisawa¹,
Masae Ikura², Tsuyoshi Ikura² and Tomonari Matsuda^{1,3}

¹Research Center for Environmental Quality Management, Kyoto University, Otsu, Shiga, Japan

²Radiation Biology Center, Kyoto University, Kyoto, Japan

Received December 26, 2013; Revised January 16, 2014; Accepted January 21, 2014
J-STAGE Advance published date: February 1, 2014

Histone H2AX phosphorylated at Ser139 (γ -H2AX) is a useful biomarker for DNA double-strand breaks. However, γ -H2AX detection has methodological disadvantages such as the requirement of expensive anti- γ -H2AX antibody and time-consuming handling for its staining. Mediator of DNA damage checkpoint 1 (MDC1) is a central adaptor protein which recruits various DNA damage response proteins to γ -H2AX and thus forms nuclear foci in the same location as γ -H2AX in response to DNA damage. Here, we describe an easy-to-use genotoxicity assay which combines enhanced green fluorescence protein (EGFP)-fused MDC1-expressing cells with a free *R* program for image-processing and quantification of foci area/nucleus. The workflow of this assay is simple: mutagen treatment, imaging, and *R*-processing. This assay does not need antibodies or staining handling and it detected the genotoxicity of a range of mutagens, including camptothecin (topoisomerase I inhibitor), cisplatin (crosslinker), and 4-nitroquinoline 1-oxide and benzo[*a*]pyrene (bulky DNA-adduct forming compounds), as increased fluorescence of EGFP-MDC1 foci. Furthermore, cotreatment with arabinofuranosyl cytosine/hydroxyurea and mutagens sensitized EGFP-MDC1 foci formation to bulky DNA adduct-type mutagens. Additionally, the established cells can be monitored in real-time using live cell imaging to obtain detailed dynamics of MDC1 in response to mutagens. The simple handling of this assay is expected to enable its full automation, thus making it useful for high-throughput genotoxicity screening of chemicals and monitoring of environmental mutagens.

Key words: MDC1, γ -H2AX, fluorescence microscopy, image-processing, *R*

Introduction

Histone H2AX phosphorylated at Ser139 (γ -H2AX) is one of the most useful biomarkers for DNA double-strand breaks (DSBs). When DSBs are induced in cells, H2AX polypeptides within about ~2 Mbp of a DSB site are phosphorylated to form γ -H2AX nuclear ag-

gregates called foci (1,2). Because a single γ -H2AX focus corresponds to one DSB (2,3), γ -H2AX is an extremely sensitive indicator for DSBs. Whereas induction of γ -H2AX was first shown in response to ionizing irradiation (1), it has since been reported that a broad spectrum of mutagens also induces γ -H2AX, including radical generators [bleomycin (4), tirapazamine (4), calicheamicin γ 1 (5), c-1027 (6), and neocarzinostatin (7)], topoisomerase inhibitors [camptothecin (CPT) (6), topotecan (8), and etoposide (4)], a DNA intercalator [doxorubicin (9)], alkylating agents [*N*-methyl-*N*-nitrosourea (MNU) (10), *N*-methyl-*N'*-nitro-*N*-nitrosoguanidine (11), adzelesin (6), methyl methanesulfonate (12), and *N*-ethyl-*N*-nitrosourea (13)], an oxidizing agent [hydrogen peroxide (7)], bulky DNA adduct-forming agents [4-nitroquinoline1-oxide (4NQO) (4), benzo[*a*]pyrene (B[*a*]P) (13), and *N*-acetoxy-2-acetylaminofluorene (13)], DNA crosslinking agents [cisplatin (CDDP) (14) and actinomycin D (15)], a ribonucleotide reductase inhibitor [hydroxyurea (HU) (16)], a DNA polymerase inhibitor [aphidicolin (17)], and a general tyrosine kinase inhibitor [staurosporine (18)]. Furthermore, the relationship between chemical dose and γ -H2AX induction is linear (4). These facts explain why there is increasing interest in using γ -H2AX as a biomarker in chemical genotoxicity assays. Indeed, previous studies have used γ -H2AX in genotoxicity assays for photogenotoxic chemicals (19,20) and for known and potential environmental pollutants such as benzene (21), polyaromatic hydrocarbons (22), nonyl-phenol polyethoxylates (23), heavy metals (24), cigarette smoke (25), and nanoparticles (26–32), and the results were all positive except for alumina (Al₂O₃) nanoparticles.

³Correspondence to: Tomonari Matsuda, Research Center for Environmental Quality Management, Kyoto University, Otsu, Shiga 5200811, Japan. Tel: +81-77-527-6224, Fax: +81-77-524-9869, E-mail: matsuda.tomonari.8z@kyoto-u.ac.jp
doi: org/10.3123/jemsge.2014.001

On the other hand, genotoxicity assays targeting γ -H2AX still have several methodological limitations. Immunofluorescence microscopy, flow cytometry, western blotting, and enzyme-linked immunosorbent assay (ELISA) are conventionally used for γ -H2AX detection, and all these methods absolutely require anti- γ -H2AX antibody, which is an expensive consumable. Furthermore, staining with γ -H2AX antibody is also burdensome and time consuming and high-throughput screening with these methods would be difficult. For environmental and chemical management applications, an easy-to-use and high-throughput method for chemical genotoxicity screening would be advantageous.

Mediator of DNA damage checkpoint 1 (MDC1) is a large protein (2,089 amino acids) (33) which plays a central role in amplification and mediation of the DNA damage response (DDR). In human cells, when a DSB occurs, the MRN complex composed of MRE11 (meiotic recombination 11)/RAD50 (homolog of *S. cerevisiae*'s Rad50)/NBS1 (Nijmegen breakage syndrome protein 1) binds to the DSB site (34), whereupon ataxia telangiectasia mutated (ATM) protein is recruited to the DNA lesion via NBS1 (35,36). ATM phosphorylates histone H2AX adjacent to the DSB site to form γ -H2AX (37). At the same time, DNA-dependent protein kinase (DNA-PK) is also recruited to the DSB site and phosphorylates H2AX (38). Subsequently, MDC1 binds to γ -H2AX (39) and brings additional ATM to the DSB site, expanding ATM-dependent H2AX phosphorylation (40). The positive feedback loop involving ATM- γ -H2AX-MDC1 amplifies DDR signaling. In the case of replication stress, ATM and rad3-related (ATR) protein phosphorylates H2AX at stalled replication forks (9,16). A recent report demonstrated that MDC1 binds to topoisomerase II binding protein 1 (TopBP1) and that both H2AX and MDC1 are required for formation of TopBP1 foci at stalled replication forks (41), suggesting a role for MDC1 in response to replication stress. By these mechanisms, MDC1 immediately (within 5 min after ionizing irradiation) forms foci in the same locations as those formed by γ -H2AX in response to DSBs (2,42).

MDC1 has multiple domains for mediating protein-protein interactions and thus functions as an important adaptor which brings and retains various DDR proteins to DSB sites through γ -H2AX. The N-terminal forkhead-associated domain interacts with Ser1981-phosphorylated ATM (40,43) and Thr68-phosphorylated checkpoint kinase 2 (Chk2) (44) in response to DSBs and constitutively with RAD51 recombinase (45); the Ser-Asp-Thr repeats constitutively phosphorylated by casein kinase 2 interact with NBS1 (46–49); the Thr-Gln-Xaa-Phe repeats phosphorylated by ATM in response to DSBs interact with ring finger protein 8 (50–52); the Pro/Ser/Thr repeats interact with DNA-PK (53); and

the tandem BRCA1 C-terminus (BRCT) domains interact with γ -H2AX (39,40), p53 (54), p53-binding protein 1 (55), cell division cycle 27 (56), murine double minute 2 (57), and Ser 1524-phosphorylated topoisomerase II α (58).

Here, we established human cells expressing enhanced green fluorescent protein (EGFP)-fused MDC1 (EGFP-MDC1) and developed an easy-to-use and rapid genotoxicity assay, which combines both the cells and a free *R* program for imaging and statistical analysis (59). We then demonstrated the efficacy of the genotoxicity assay by testing several different types of mutagens, including the DNA topoisomerase inhibitor CPT, the crosslinking agent CDDP, the bulky adduct-forming compounds 4NQO and B[a]P, and the alkylating agent MNU.

Materials and Methods

Chemicals: Dimethyl sulfoxide (DMSO), MNU, arabinofuranosyl cytosine (AraC) and HU were purchased from Wako (Osaka, Japan). CDDP and CPT were purchased from Sigma-Aldrich (Missouri, USA). 4NQO and B[a]P were purchased from Nacalai Tesque (Kyoto, Japan). *O*⁶-benzylguanine (*O*⁶-BG) was purchased from Santa Cruz (California, USA). The chemicals were dissolved in DMSO.

Cell culture: Human breast adenocarcinoma MCF7 cells were cultured in Dulbecco's Modified Eagle's Medium supplemented with 10% fetal bovine serum at 37°C in a humidified 5% CO₂ incubator.

Construction of pEGFP-C1/MDC1 plasmid: First, the middle region of human *MDC1* cDNA (K1AA0170) were cut out with *Hind*III and *Eco*RI and inserted into the same sites of pEGFP-C1 vector (Clontech, California, USA) (pEGFP-C1/MDC1 Δ N Δ C). Next, the 3' terminus region of human *MDC1* was amplified from human *MDC1* cDNA by polymerase chain reaction (PCR) with the following primers: 3' terminus MDC1-F, 5'-ccggaattccaatctctgtcaccacagaccag-3' (an *Eco*RI site is underlined); 3' terminus MDC1-R, 5'-tcccgcggctcaggtgatgacatctccaaagggg-3' (a *Sac*II site is underlined). The PCR product was cut with *Eco*RI and *Sac*II and inserted into pEGFP-C1/MDC1 Δ N Δ C cut with the same restriction enzymes (pEGFP-C1/MDC1 Δ N). Subsequently, the 5' terminus region of human *MDC1* was amplified from human *MDC1* cDNA by PCR with the following primers: 5' terminus MDC1-F, 5'-ccc aagcttccgaggacaccaggtattgactgg-3' (a *Hind*III site is underlined); 5' terminus MDC1-R, 5'-cccaagcttggcttttctcagaggacagcc-3' (a *Hind*III site is underlined). The PCR product was cut with *Hind*III and inserted into pEGFP-C1/MDC1 Δ N cut with the same restriction enzyme (pEGFP-C1/MDC1).

Transduction of stable EGFP-MDC1-expressing MCF7 (EGFP-MDC1/MCF7) cells: pEGFP-C1/MDC1 was transfected into MCF7 cells by Lipofecta-

mine 2000 (Life technologies, California, USA) according to the manufacturer's protocol. After 48 h, stable transformants were selected using medium supplemented with 1 mg/ml G418.

Immunoprecipitation: Cells grown to 80% confluence in 100 mm dishes were suspended into 1 mL ice-cold phosphate-buffered saline (PBS) (137 mM NaCl, 2.68 mM KCl, 8.10 mM Na_2HPO_4 , and 1.67 mM NaH_2PO_4) and pelleted by centrifugation at 1,000 rpm for 1 min at 4°C. Cell pellets were resuspended in 1 mL ice-cold cell lysis buffer (150 mM NaCl, 10 mM Tris-HCl pH 7.3, 0.5 mM ethylenediaminetetraacetic acid, 1 mM beta-mercaptoethanol, 0.2 mM phenylmethylsulfonyl fluoride, 10 mM beta-glycerophosphate, and 1% NP-40) and incubated for 20 min on ice. Lysate was centrifuged at 15,000 rpm for 15 min at 4°C. 65 μL of the supernatant was saved as a whole-cell lysate (Input) sample and the remaining supernatant was used for immunoprecipitation. 1 μL anti-GFP antibody (ab290, Abcam, Cambridge, UK) was added to the supernatant and the sample was rotated for 60 min at 4°C. Next, after addition of 20 μL of a 50% slurry of Protein A agarose (Merck Millipore, Massachusetts, USA), the sample was rotated for 60 min at 4°C. The sample was pelleted by centrifugation at 8,000 rpm for 1 min at 4°C. Pellets were washed with 500 μL ice-cold cell lysis buffer three times and then analyzed by Western blotting as immunoprecipitated (IP) samples.

Western blotting: Input or IP sample was denatured in NuPAGE LDS Sample Buffer (Life technologies) at 70°C for 10 min. For IP samples, each sample was pelleted by centrifugation at 15,000 rpm for 1 min and the supernatant was diluted ten-fold with NuPAGE LDS Sample Buffer. To separate proteins, 3 μL /sample was applied to each well of a NuPAGE Novex 4–12% Bis-Tris Gel (Life technologies) and electrophoresis was performed in NuPAGE MES SDS Running Buffer (Life technologies) at 200 V for 60 min. Separated proteins were blotted onto Hybond ECL membrane (GE Healthcare, Buckinghamshire, UK) by electrophoresis (100 V for 90 min in blotting buffer (20% methanol, 25 mM Tris, and 192 mM glycine)). The membrane was incubated for 60 min with 5% skimmed milk in TBS-T (137 mM NaCl, 20 mM Tris-HCl pH 7.6, 0.1% Tween 20) for blocking. Next, the membrane was incubated for 60 min with anti-MDC1 antibody (1:1,000) (ab11169, Abcam) or anti-GFP antibody (1:1,000) (ab290, Abcam) in TBS-T. Subsequently, the membrane was incubated for 60 min with horseradish peroxidase-conjugated goat anti-rabbit antibody (1:10,000) (#7074, Cell Signaling Technology, Massachusetts, USA) in TBS-T. To develop chemiluminescence by horseradish peroxidase, the membrane was incubated for 5 min with ECL Prime WB Detection Reagent (GE Healthcare). Chemiluminescence detection was performed using an

LAS-1000 image analyzer controlled by Image Reader LAS-1000 Mini V1.21 software (Fujifilm, Tokyo, Japan).

Immunofluorescence staining and microscopy:

For immunofluorescence staining, EGFP-MDC1-expressing MCF7 cells (2×10^5) were seeded onto a 24×24 mm² cover glass (Matsunami glass, Osaka, Japan) in each well of a 6-well plate and treated with 10 μM CPT for 1 h. CPT dissolved in DMSO were added to the medium directly and the final DMSO concentration was 0.1% (v/v). After experimental treatment, subsequent incubation was performed in the dark as much as possible. Cells were fixed with 4% formaldehyde in PBS for 10 min and permeabilized with 0.2% Triton X-100 in PBS for 10 min. Next, cells were incubated in 4% bovine serum albumin in PBS for 30 min for blocking. Cells were incubated for 60 min with anti-MDC1 antibody (1:100) (ab11169) or anti- γ -H2AX antibody (1:100) (a component of the OxiSelect DNA Double Strand Break (DSB) Staining Kit, Cell Biolabs, California, USA) in 1% BSA in PBS. As a negative control, an equal concentration of normal rabbit IgG (sc-2027, Santa Cruz) or normal mouse IgG (sc-2025, Santa Cruz) diluted with 1% BSA in PBS was used. Subsequently, cells were incubated for 60 min with tetramethylrhodamine-5-(and 6)-isothiocyanate (TRITC)-conjugated goat anti-rabbit (1:200) (ab6718, Abcam) or TRITC-conjugated goat anti-mouse IgG (ab7065, Abcam). Nuclei were stained for 10 min with 0.5 $\mu\text{g}/\text{mL}$ Hoechst 33342. Microscopic observations were performed using a BZ-9000 fluorescence microscope (Keyence, Osaka, Japan). A $20 \times$ (Plan Apo/0.75 numerical aperture) objective was used. Image processing was performed by using a BZ-II Analyzer (Keyence).

Programming in R: After microscopic imaging, TIF-images were converted to JPG-images using BZ-II Resizer (Keyence) to reduce file sizes. Image-processing and statistical analysis were processed in R, and image-processing was performed using the EBImage package (60). JPG-images for each individual treatment were separately placed into different R-work folders. Workflow of the program using R is shown in Fig. 2A. The detailed program was described in supplemental information (Available at <https://www.jstage.jst.go.jp/browse/jemsge>). Briefly, green channels of the EGFP-MDC1 images were converted to gray scale images, brightness of the images was normalized, and nuclei and foci were separately extracted from the same normalized images. In nuclear extraction, the images were binarized and the resulting sets of combined pixels (named objects) were numbered. Based on thresholds of area and acircularity of each object and mean brightness of each nucleus corresponding to each object, noise (objects not corresponding to any nuclei in the normalized images) and objects corresponding to nuclei with weak bright-

ness were removed. In foci extraction, the normalized images were binarized using the different condition from that of nuclear extraction. Finally, total foci area/nucleus was calculated using the extracted nuclei and foci images.

A new genotoxicity assay: EGFP-MDC1/MCF7 cells (2×10^5) seeded in 35-mm glass-base dishes were treated with mutagens for various times. The mutagens dissolved in DMSO were added to the medium directly and the maximum of final DMSO concentration was 0.25% (v/v). In the AraC/HU co-treatment experiment, the final DMSO concentration was 0.4% (v/v). In the O6-BG co-treatment experiment, the final DMSO concentration was 0.35% (v/v). Cells were fixed with 4% formaldehyde in PBS for 10 min. After a PBS wash, microscopic observations were performed. A 20 \times (Plan Apo/0.75 numerical aperture) objective and the quick full-focus function were used. In each experimental condition, 10–15 different fields were imaged and image-processing and calculation of foci area/nucleus were

performed using *R*.

Results

To establish EGFP-MDC1/MCF7 cells, pEGFP-C1/MDC1 was transfected into MCF7 cells. Although stable transformants had been selected by G418, the population of EGFP-MDC1-expressing cells observed by fluorescence microscopy was very small (about 1%), but cells with a strong EGFP signal were isolated. To confirm that full-length EGFP-MDC1 was expressed in the isolated cells, western blotting (WB) following immunoprecipitation (IP) with anti-GFP antibody was performed (Fig. 1A). In the input sample, anti-MDC1 antibody detected endogenous MDC1 signal located at about 220 kDa in both EGFP-MDC1-transduced cells and negative control cells, whereas an additional MDC1 signal corresponding to a protein larger than endogenous MDC1 was detected only in EGFP-MDC1-transduced cells. The difference in sizes between the endogenous and the larger MDC1 corresponds to the size

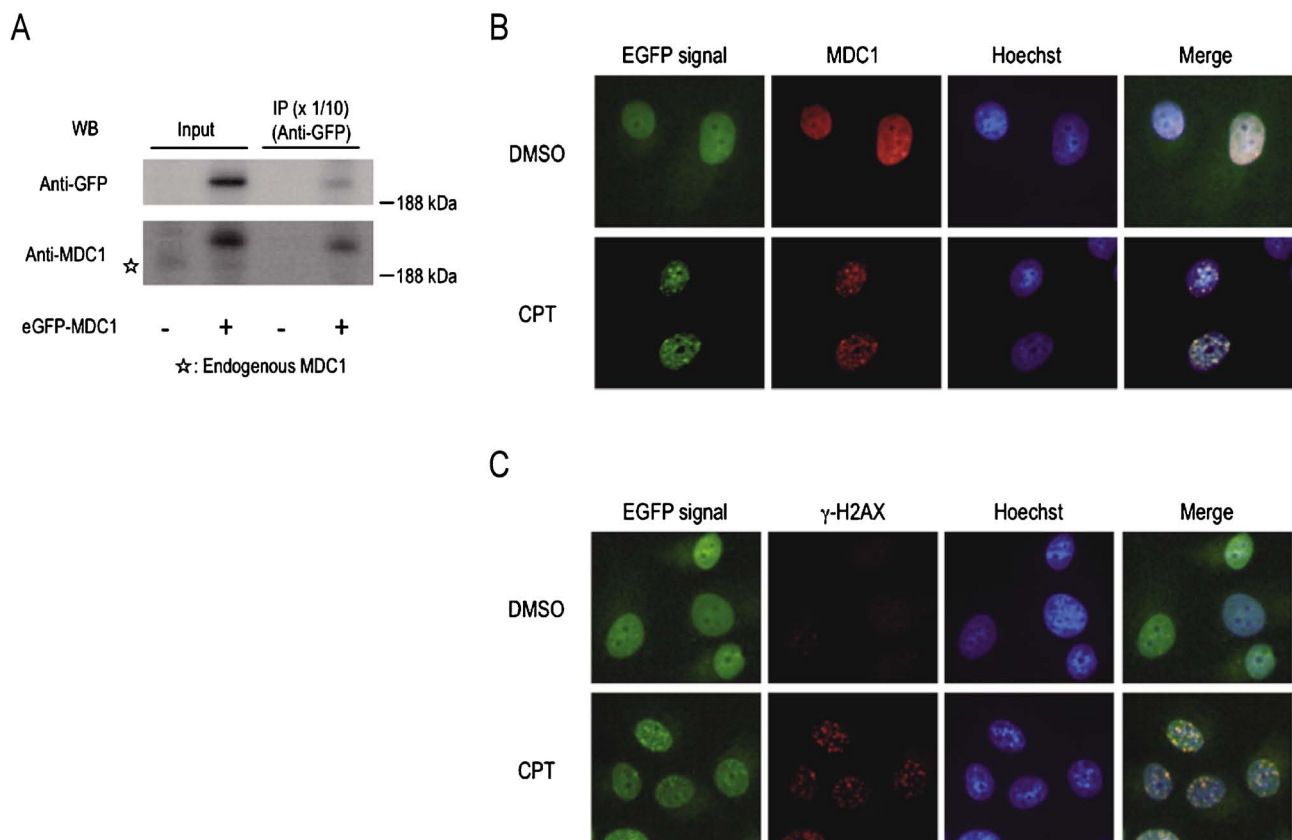
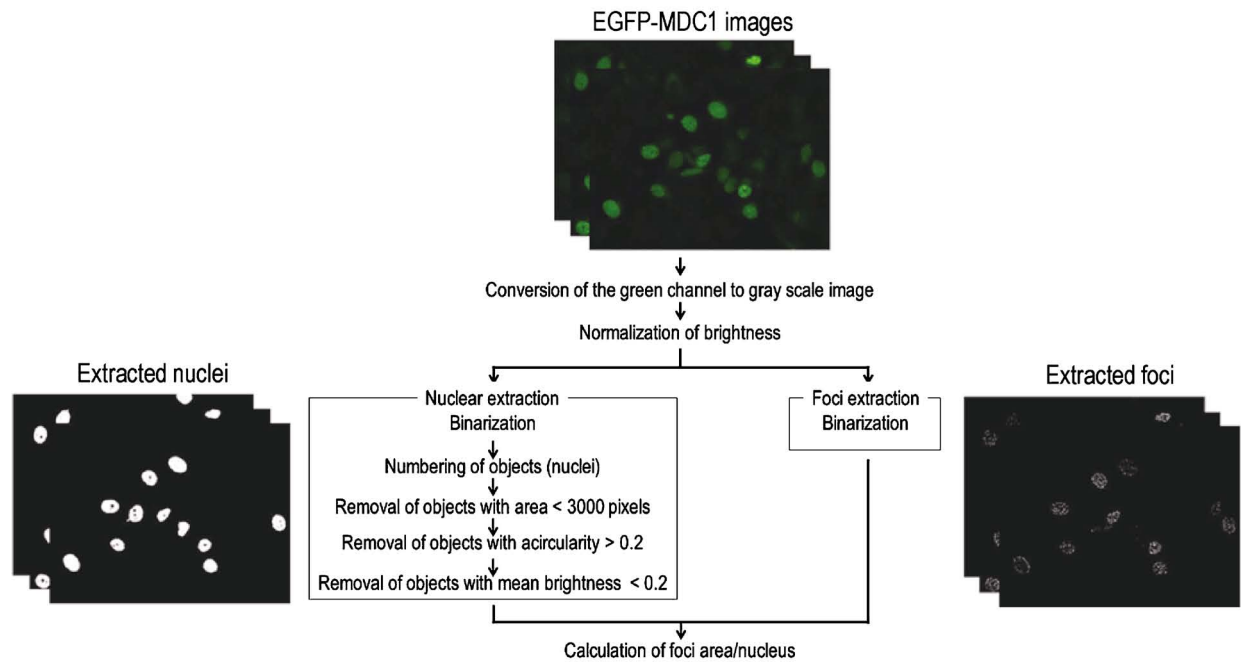


Fig. 1. (Color online) Establishment of EGFP-MDC1-expressing MCF7 cells. (A) Expression of EGFP-MDC1 in human breast adenocarcinoma MCF7 cells. Cells were transduced with pEGFP-C1/MDC1 plasmids. After G418 selection, the cells were lysed, immunoprecipitated with anti-GFP antibody, and the precipitates were subjected to western blotting using anti-GFP or anti-MDC1 antibodies. The opened star indicates bands corresponding to endogenous MDC1. (B) EGFP signal forms foci in response to DNA damage and colocalizes with MDC1. After treatment for 1 h with 0.1% (v/v) DMSO (vehicle control) or 10 μ M camptothecin (CPT), EGFP-MDC1/MCF7 cells were immunostained with anti-MDC1 antibody. (C) EGFP signal colocalizes with γ -H2AX. After treatment for 1 h with 0.1% (v/v) DMSO (vehicle control) or 10 μ M CPT, EGFP-MDC1/MCF7 cells were immunostained with anti- γ -H2AX antibody.

A



B

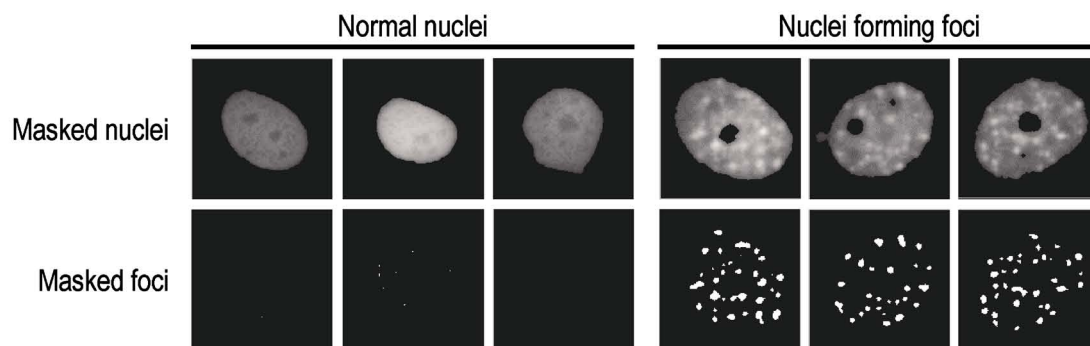


Fig. 2. (Color online) Workflow of image-processing using *R*. (A) Workflow of the program using *R*. After EGFP-MDC1 imaging, nuclei and foci were separately masked from the same EGFP-MDC1 image and then the masked foci area in each masked nucleus was calculated. (B) Representative images of masked nuclei and masked foci of normal nuclei and nuclei forming foci.

of EGFP (about 27 kDa). Using anti-GFP antibody, GFP signal was detected only in EGFP-MDC1-transduced cells, and the band was located at the same size as the upper MDC1-signal. After IP with anti-GFP antibody, both GFP and MDC1 signals were detected only in EGFP-MDC1-transduced cells and their locations corresponded to that of the larger MDC1. These results clearly show that full-length EGFP-MDC1 was expressed in EGFP-MDC1-transduced cells and the level of EGFP-MDC1 expression was much higher than that of endogenous MDC1.

We tested whether EGFP-MDC1 expressed in the established EGFP-MDC1/MCF7 cells was functional. Cells were treated with DMSO (negative control) or 10 μ M CPT for 1 h and immunofluorescence analysis using anti-MDC1 and anti- γ -H2AX antibody was performed.

As shown in Fig. 1B, immunostaining with anti-MDC1 antibody produced a diffuse nuclear signal in DMSO-treated cells but revealed discrete foci in nuclei in response to CPT. Localization of GFP signal completely overlapped with that of the anti-MDC1 signal. Similarly, the signal from anti- γ -H2AX antibody was observed as discrete foci and increased in response to CPT (Fig. 1C). Foci identified by GFP signal overlapped with the anti- γ -H2AX signal. Given these facts, we confirmed that EGFP-MDC1 expressed in EGFP-MDC1/MCF7 cells was functional, at least to the extent that EGFP-MDC1 localizes to nuclear foci in response to DNA damage.

Next, to quantify EGFP-MDC1 formation after mutagen treatment, we developed an automated program for image-processing using *R*. The outline of the

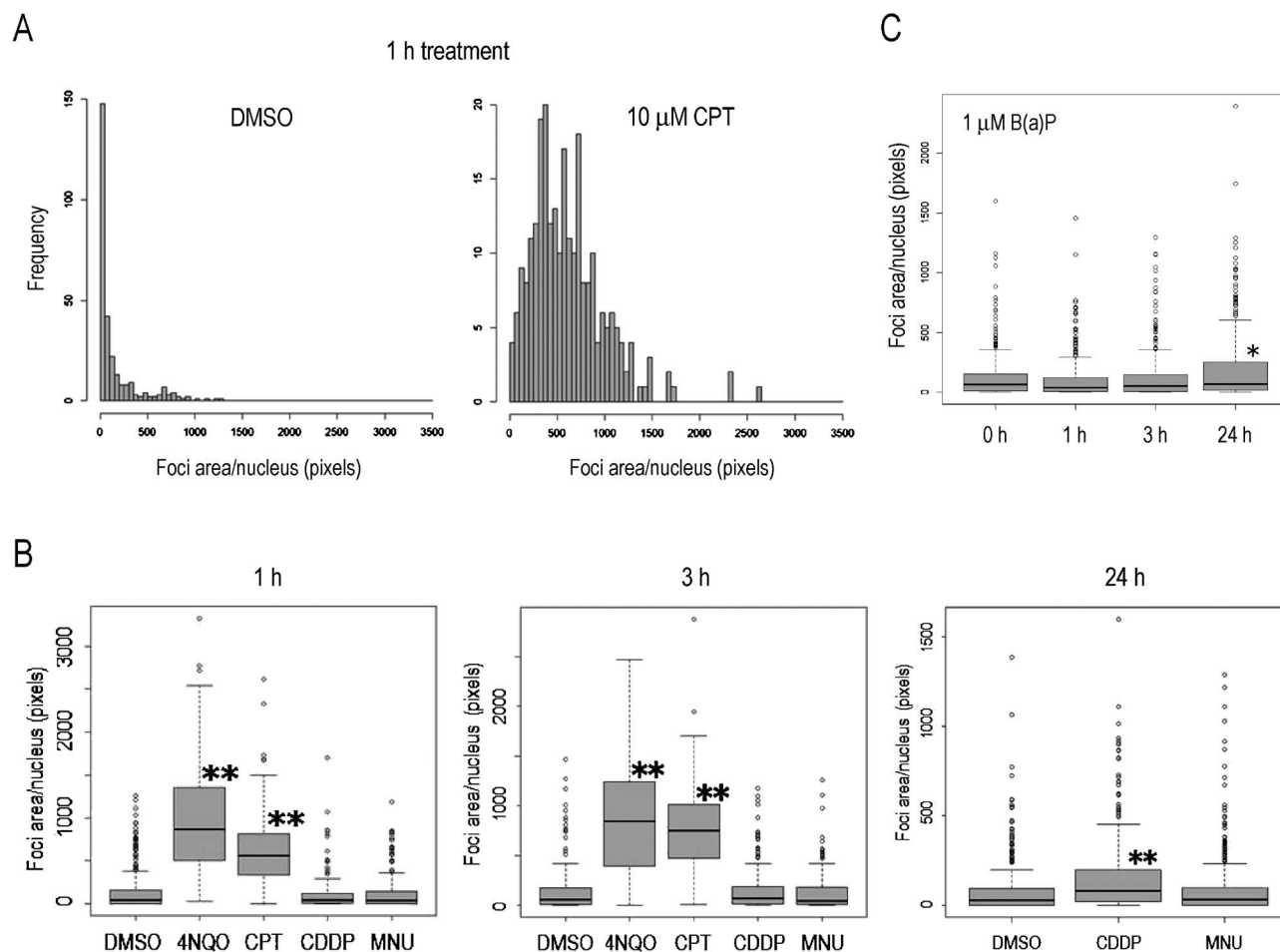


Fig. 3. Results of mutagen tests using the new genotoxicity assay. (A) Representative histograms of EGFP-MDC1 foci area/nucleus of EGFP-MDC1/MCF7 cells treated for 1 h with 0.1% (v/v) DMSO (control) or 10 μ M CPT (damage). (B) Boxplots of foci area/nucleus for each condition. After EGFP-MDC1/MCF7 cells were treated for 1, 3, or 24 h with 0.25% (v/v) DMSO (vehicle control), 10 μ M 4NQO, 10 μ M CPT, 40 μ M CDDP, or 1 mM MNU, the new genotoxicity assay was performed. 200–490 cells were counted for each condition. (C) Boxplots of foci area/nucleus of EGFP-MDC1/MCF7 cells treated with B[a]P. EGFP-MDC1/MCF7 cells were either left untreated (0 h) or treated for 1, 3, or 24 h with 1 μ M B[a]P, and the new genotoxicity assay was performed. 271–432 cells were counted for each condition. * $p < 0.0001$ versus 0 h, ** $p < 1.0 \times 10^{-12}$ versus DMSO, Wilcoxon signed-rank test, respectively.

procedure is shown in Fig. 2A, and works as follows. After mutagen treatment, GFP signal in the cells is imaged by immunofluorescence microscopy with vivid clarity. Then, each nucleus area and focus area are separately extracted from the same image (Fig. 2B), each focus is linked to its corresponding nucleus, and total foci area in each nucleus is calculated using *R*. The details of the procedure are described in Materials and Methods. Furthermore, we carefully optimized the condition of the image-processing conditions of the program.

Using EGFP-MDC1/MCF7 cells and the image-processing program, we established a new genotoxicity assay. The workflow is simple: sample treatment, fixation (if required), microscopic imaging, and image-processing and calculation of foci area/nucleus using *R*. We applied the genotoxicity assay to four types of muta-

gens: CPT (topoisomerase I inhibition), 4NQO (bulky DNA-adduct formation), CDDP (DNA crosslinking), and MNU (DNA alkylation). EGFP-MDC1/MCF7 cells were treated with 10 μ M CPT, 10 μ M 4NQO, 40 μ M CDDP, or 1 mM MNU for 1, 3, or 24 h, and the genotoxicity assay was performed. Representative and all histograms of EGFP-MDC1 foci area/nucleus of normal and damaged cells are shown in Fig. 3A and Supplemental Fig. 1, clearly illustrating that most DMSO-treated (control) cells have relatively small EGFP-MDC1 foci areas whereas most CPT-treated (damaged) cells have extensive foci areas. As shown in Fig. 3B, CPT or 4NQO exposure significantly increased the area of EGFP-MDC1 foci after 1 h whereas no obvious changes were detected after CDDP or MNU treatment at 1 h. However, CDDP treatment significantly increased the area of EGFP-MDC1 foci after 24 h. On the

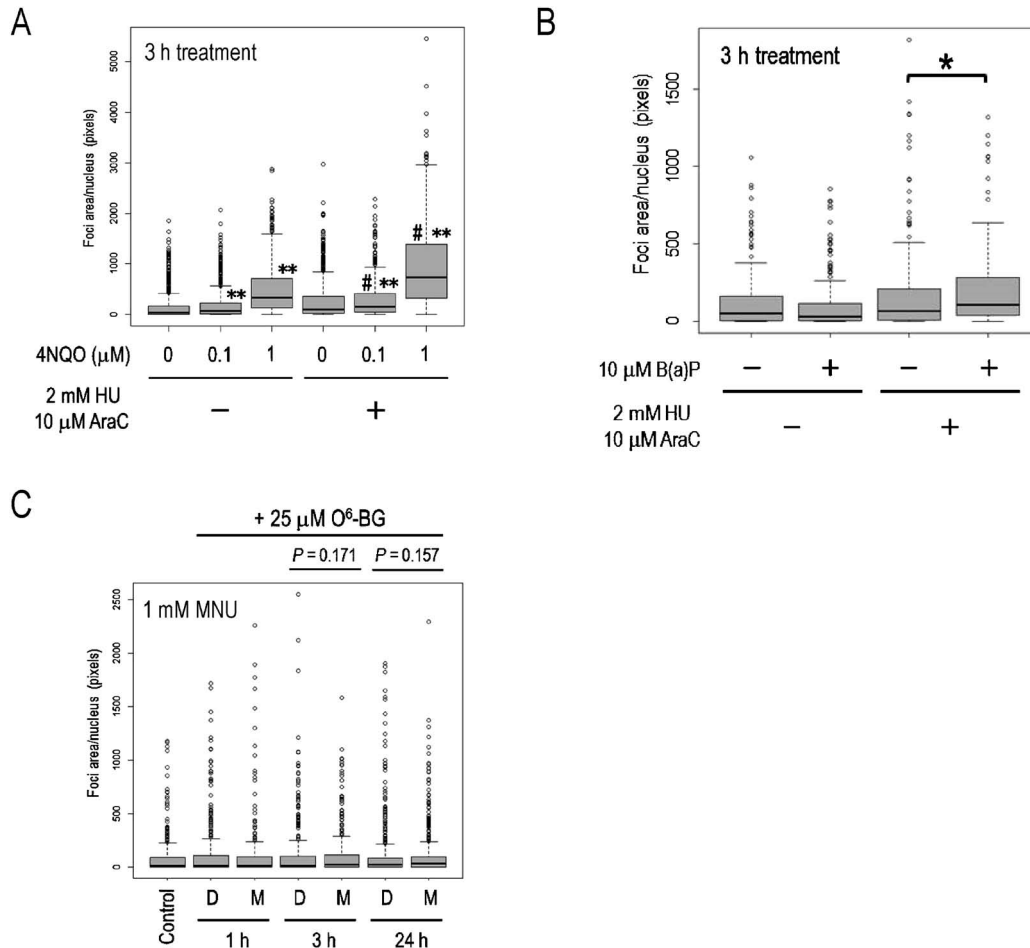


Fig. 4. Enhancement of EGFP-MDC1 foci formation. (A) Boxplots of foci area/nucleus of EGFP-MDC1/MCF7 cells cotreated with 4NQO and AraC/HU. After EGFP-MDC1/MCF7 cells were cotreated for 3 h with 10 μM AraC/2 mM HU and 0 (0.1% (v/v) DMSO, vehicle control), 0.1 or 1 μM 4NQO, the new genotoxicity assay was performed. 783–1069 cells were counted for each condition. (B) Boxplots of foci area/nucleus of EGFP-MDC1/MCF7 cells cotreated with B[a]P and AraC/HU. EGFP-MDC1/MCF7 cells were cotreated for 3 h with 10 μM AraC/2 mM HU and 0.1% (v/v) DMSO (vehicle control) or 10 μM B[a]P, and the new genotoxicity assay was performed. 189–204 cells were counted for each condition. (C) Boxplots of foci area/nucleus of EGFP-MDC1/MCF7 cells cotreated with MNU and O^6 -BG. EGFP-MDC1/MCF7 cells were untreated (Control) or cotreated for 1, 3, or 24 h with 25 μM O^6 -BG and 0.25% (v/v) DMSO (vehicle control) (D) or 1 mM MNU (M), and the new genotoxicity assay was performed. 290–633 cells were counted for each condition. * $p < 0.05$, ** $p < 1.0 \times 10^{-12}$ versus DMSO, # $p < 1.0 \times 10^{-12}$ versus the same concentration of 4NQO without AraC/HU, Wilcoxon signed-rank test, respectively.

other hand, MNU did not increase the area of EGFP-MDC1 foci after 24 h, the longest time point examined. Next, we tested B[a]P which requires metabolic activation to form bulky DNA adducts. Whereas no increase in the area of EGFP-MDC1 foci was observed in 1 μM B[a]P-treated cells at 1 h and 3 h, a significant increase was observed 24 h after treatment (Fig. 3C).

To enhance the sensitivity of EGFP-MDC1/MCF7 cells to mutagens, AraC (DNA polymerase inhibitor) and HU were co-administered with 4NQO or B[a]P. In 4NQO-treated cells, co-treatment with AraC and HU significantly increased the EGFP-MDC1 foci area (Fig. 4A). In the case of B[a]P, although significant EGFP-MDC1 foci formation requires 24 h of treatment (Fig. 3C and 4B), co-treatment with AraC and HU sig-

nificantly increased EGFP-MDC1 formation after only 3 h treatment (Fig. 4B). In an attempt to enhance the sensitivity of EGFP-MDC1/MCF7 cells to MNU, which was negative in the genotoxicity assay (Fig. 3B), 25 μM O^6 -BG was co-administered with MNU. MNU forms alkylated DNA lesions such as O^6 -methylguanine (O^6 -MG) and O^6 -BG is an inhibitor of O^6 -methylguanine DNA methyltransferase (MGMT) which repairs O^6 -MG back to guanine. As shown in Fig. 4C, co-treatment with MNU and O^6 -BG increased EGFP-MDC1 foci formation at both 3 h and 24 h treatment but the increase was not significant.

Discussion

Here, we established an easy-to-use genotoxicity as-

say which combines EGFP-MDC1/MCF7 cells with an automated image-processing program using *R* software. This assay has several advantages compared with other genotoxicity assays targeting γ -H2AX. First, our method does not need any antibodies, which are expensive consumables, whether obtained commercially or prepared in house. Second, our method does not require any staining procedures and thus saves on staining and handling time. Third, the assay accommodates live cell imaging, which enables detection of not only EGFP-MDC1 foci formation but also its detailed dynamic changes in terms of location, size, shape and brightness. CPT, 4NQO, CDDP, and B[a]P are all known inducers of DSBs and γ -H2AX (4,6,13,14,61–64), and all induced EGFP-MDC1 foci in our new genotoxicity assay (Fig. 3). These results suggest that our assay can detect genotoxicity of a range of mutagens.

CPT forms a stable complex with topoisomerase I (Topo I) and DNA to inhibit Topo I (65) and induces a DSB specifically affecting the leading strand of the replication fork in S phase of the cell cycle (61). However, we observed that EGFP-MDC1 foci formed in most cells treated with CPT (data not shown), suggesting that CPT may also induce DSBs at stages other than S phase. Consistent with this possibility, it was reported that CPT also forms a stable CPT-Topo I-DNA complex during transcription (66) and induces DSBs and γ -H2AX in post-mitotic cells (67).

4NQO also induces DSBs (62) and the frequency is not changed through the cell cycle (4). This fact is consistent with our observation that EGFP-MDC1 foci were formed in most cells treated with 4NQO as well as CPT (data not shown). On the other hand, 4NQO most significantly induces γ -H2AX foci in S phase (4), implying that it generates DNA lesions other than DSBs which also induce γ -H2AX and MDC1 foci. One possibility is that stalled replication forks unaccompanied by DSBs result in foci formation. It was shown that bulky DNA adducts formed by 4NQO induce stalling of replication forks in yeasts (68) and that stalling of replication forks by mutagens induces ATR-dependent γ -H2AX and MDC1 foci (16,41). However, at least to our knowledge, it is still unclear what (DSBs, single-strand breaks, or others?) actually induces γ -H2AX and MDC1 foci at stalled replication forks.

Bulky DNA adducts formed by mutagens such as 4NQO, B[a]P, and ultraviolet (UV) irradiation are repaired by nucleotide excision repair (NER) (69–72). NER is a multistep process that consists of recognition of a DNA lesion, unwinding of the DNA helix around the lesion, dual incision around the lesion, excision of 24–32 nucleotides around the lesion, and gap-filling DNA synthesis (73). γ -H2AX can also be induced in cells in G₀/G₁ phase in an NER-dependent manner. In this case, H2AX phosphorylation depends not on ATM

or DNA-PK but on ATR (74,75). After UV irradiation or treatment with N-acetoxy-2-acetylaminofluorene, which also forms bulky DNA adducts (76), γ -H2AX in G₀/G₁ phase is reduced in NER-defective cells such as xeroderma pigmentosum (XP)-A, XP-C, or XP-G cells, which are defective in formation of the pre-incision complex, recognition of DNA damage, and cleavage on the 3' side of the damaged DNA, respectively (74,75,77). Consistent with this, ectopic expression of wild-type XPA in XP-A cells recovers the γ -H2AX induction in G₀/G₁ phase after UV irradiation (74). Furthermore, the γ -H2AX in G₀/G₁ phase after UV irradiation is increased by DNA polymerase inhibition with aphidicolin, AraC, or AraC/HU treatment, suggesting that the DNA single-strand gaps formed during NER could eventually induce γ -H2AX (74,75). We previously utilized AraC/HU for sensitization of DNA strand break detection in a fluorometric analysis of DNA unwinding assay (78). These observations motivated us to test whether AraC/HU treatment would promote EGFP-MDC1 foci formation by bulky DNA adduct-forming mutagens which are repaired through NER. In fact, AraC/HU treatment increased and accelerated EGFP-MDC1 foci formation in 4NQO-treated and B[a]P-treated cells, respectively (Fig. 4), suggesting that AraC/HU could sensitize our assay to mutagens repaired through NER. Furthermore, our results strongly indicate that MDC1 participates not only in the cellular responses to DSBs and stalling of replication forks, but also in NER-mediated repair. However, it is unclear whether γ -H2AX/MDC1 foci respond to DNA single-strand gaps or the resultant DSB lesions. If γ -H2AX/MDC1 foci directly respond to the former, then whether γ -H2AX/MDC1 foci formation is a general process in NER will need to be elucidated in further studies.

MNU is a simple alkylating mutagen, and one of major DNA lesions induced by MNU is O⁶-MG (79). MGMT repairs O⁶-MG to guanine by removing the methyl adduct of the base (80,81). In this case, any DNA single-strand gaps would not occur and thus there would be no opportunity for γ -H2AX/MDC1 foci induction as in NER. Our result, that MNU treatment did not increase EGFP-MDC1 foci (Fig. 3B), implies an important role for the MGMT repair system. Indeed, MGMT-defective cells induce γ -H2AX in response to MNU (10). These facts encouraged us that MGMT inhibition might sensitize our assay to MNU, and therefore we used the MGMT inhibitor O⁶-BG (82) for this purpose. O⁶-BG binds to MGMT by competing with O⁶-MG and transfers its benzyl group to MGMT, resulting in irreversible inhibition of MGMT (83). As shown in Fig. 4C, co-treatment with MNU and O⁶-BG increased the area of EGFP-MDC1 foci but the increase was not significant. It remains a possibility that optimization of O⁶-BG treatment conditions such as O⁶-BG concentra-

tion and timing could improve the sensitivity of our assay to MNU. A major repair system of *O*⁶-MG other than MGMT is mismatch repair (MMR) (84,85). Since MMR causes single-strand gaps through repair similar to NER (86), gaps may induce γ -H2AX through MMR as well as through NER.

As is well known, B[a]P requires metabolic activation for genotoxicity expression (87). In cells, B[a]P activates the transcription factor aryl hydrocarbon receptor which subsequently increases expression of xenobiotic metabolizing enzymes such as cytochrome P450 (CYP) 1A1 and CYP1A2 (88,89). These enzymes metabolize B[a]P to produce benzo(a)pyrene diol epoxide (BPDE) which forms a bulky DNA adduct (70,90). Thus, there is a time lag between enzyme induction and bulky DNA-adduct formation after B[a]P treatment (Supplemental Fig. 2). This is consistent with our data, that B[a]P needed 24 h to induce significant EGFP-MDC1 foci formation whereas the direct mutagen 4NQO required only 1 h (Fig. 3). Furthermore, this result indicates that the assay can utilize the bioactivation processes of the human cells and thus can detect genotoxicity of some indirect mutagens without supplementary metabolic activation although whether the cells sufficiently express all kinds of metabolic enzymes has not been tested.

Some mutagens such as UV can induce not only γ -H2AX foci but also pan-nuclear distribution of γ -H2AX (91). The image-processing program of our genotoxicity assay may not detect the latter response as positive and thus may underestimate the genotoxicity of some mutagens although we have not tested such mutagens yet. Recent report showed that MDC1 binds to ionizing irradiation-induced pan-nuclear γ -H2AX, clearly indicating involvement of MDC1 in DDR by pan-nuclear γ -H2AX (92). A detailed observation of cells to detect a change in localization of EGFP-MDC1 between normal and pan-nuclear γ -H2AX-forming cells would be required in a further study for improvement of our genotoxicity assay.

The protocol of our assay is simple (mutagen treatment, microscopic imaging, and image-processing and calculation of foci area/nucleus using *R*). Therefore, we are confident that automation of all the steps can be achieved and thus our assay can be applied to high-throughput genotoxicity screening and monitoring of environmental mutagens.

Acknowledgements: This study was supported by KAKENHI (23221006) from JSPS, Grant-in-Aid for JSPS Fellows (24–5844), and Grant-in-Aid for Scientific Research on Innovative Areas “Coupling of replication, repair and transcription, and their common mechanism of chromatin remodeling” from JSPS.

Conflicts of interest: The authors declare no conflict of

interest.

References

- 1 Rogakou EP, Pilch DR, Orr AH, Ivanova VS, Bonner WM. DNA double-stranded breaks induce histone H2AX phosphorylation on serine 139. *J Biol Chem*. 1998; 273: 5858–68.
- 2 Rogakou EP, Boon C, Redon C, Bonner WM. Megabase chromatin domains involved in DNA double-strand breaks in vivo. *J Cell Biol*. 1999; 146: 905–16.
- 3 Rothkamm K, Lobrich M. Evidence for a lack of DNA double-strand break repair in human cells exposed to very low x-ray doses. *Proc Natl Acad Sci USA*. 2003; 100: 5057–62.
- 4 Banath JP, Olive PL. Expression of phosphorylated histone H2AX as a surrogate of cell killing by drugs that create DNA double-strand breaks. *Cancer Res*. 2003; 63: 4347–50.
- 5 Elmroth K, Nygren J, Martensson S, Ismail IH, Hammarsten O. Cleavage of cellular DNA by calicheamicin gamma1. *DNA Repair (Amst)*. 2003; 2: 363–74.
- 6 Liu JS, Kuo SR, Beerman TA, Melendy T. Induction of DNA damage responses by adozelesin is S phase-specific and dependent on active replication forks. *Mol Cancer Ther*. 2003; 2: 41–7.
- 7 Noel G, Giocanti N, Fernet M, Megnin-Chanet F, Favaudon V. Poly (ADP-ribose) polymerase (PARP-1) is not involved in DNA double-strand break recovery. *BMC Cell Biol*. 2003; 4: 7.
- 8 Huang X, Traganos F, Darzynkiewicz Z. DNA damage induced by DNA topoisomerase I- and topoisomerase II-inhibitors detected by histone H2AX phosphorylation in relation to the cell cycle phase and apoptosis. *Cell Cycle*. 2003; 2: 614–9.
- 9 Hammond EM, Dorie MJ, Giaccia AJ. ATR/ATM targets are phosphorylated by ATR in response to hypoxia and ATM in response to reoxygenation. *J Biol Chem*. 2003; 278: 12207–13.
- 10 Komori K, Takagi Y, Sanada M, Lim TH, Nakatsu Y, Tsuzuki T, et al. A novel protein, MPO1, that functions in apoptosis triggered by O6-methylguanine mispair in DNA. *Oncogene*. 2009; 28: 1142–50.
- 11 Stojic L, Mojas N, Cejka P, Di Pietro M, Ferrari S, Marra G, et al. Mismatch repair-dependent G2 checkpoint induced by low doses of SN1 type methylating agents requires the ATR kinase. *Genes Dev*. 2004; 18: 1331–44.
- 12 Liu JS, Kuo SR, Melendy T. Comparison of checkpoint responses triggered by DNA polymerase inhibition versus DNA damaging agents. *Mutat Res*. 2003; 532: 215–26.
- 13 Zhou C, Li Z, Diao H, Yu Y, Zhu W, Dai Y, et al. DNA damage evaluated by gammaH2AX foci formation by a selective group of chemical/physical stressors. *Mutat Res*. 2006; 604: 8–18.
- 14 Huang X, Okafuji M, Traganos F, Luther E, Holden E, Darzynkiewicz Z. Assessment of histone H2AX phosphorylation induced by DNA topoisomerase I and II inhibitors topotecan and mitoxantrone and by the DNA cross-linking agent cisplatin. *Cytometry A*. 2004; 58:

- 99–110.
- 15 Mischo HE, Hemmerich P, Grosse F, Zhang S. Actinomycin D induces histone gamma-H2AX foci and complex formation of gamma-H2AX with Ku70 and nuclear DNA helicase II. *J Biol Chem.* 2005; 280: 9586–94.
- 16 Ward IM, Chen J. Histone H2AX is phosphorylated in an ATR-dependent manner in response to replicational stress. *J Biol Chem.* 2001; 276: 47759–62.
- 17 Hammond EM, Green SL, Giaccia AJ. Comparison of hypoxia-induced replication arrest with hydroxyurea and aphidicolin-induced arrest. *Mutat Res.* 2003; 532: 205–13.
- 18 Andreau K, Castedo M, Perfettini JL, Roumier T, Pichart E, Souquere S, et al. Preapoptotic chromatin condensation upstream of the mitochondrial checkpoint. *J Biol Chem.* 2004; 279: 55937–45.
- 19 Toyooka T, Ishihama M, Ibuki Y. Phosphorylation of histone H2AX is a powerful tool for detecting chemical photogenotoxicity. *J Invest Dermatol.* 2011; 131: 1313–21.
- 20 Toyooka T, Ibuki Y. Co-exposure to benzo[a]pyrene and UVA induces phosphorylation of histone H2AX. *FEBS Lett.* 2005; 579: 6338–42.
- 21 Ishihama M, Toyooka T, Ibuki Y. Generation of phosphorylated histone H2AX by benzene metabolites. *Toxicol In Vitro.* 2008; 22: 1861–8.
- 22 Shimohara C, Sawai T, Yagi T. Polyaromatic hydrocarbons cause histone H2AX phosphorylation in the S-phase of the cell cycle. *Genes Environ.* 2008; 30: 92–9.
- 23 Toyooka T, Kubota T, Ibuki Y. Nonylphenol polyethoxylates induce phosphorylation of histone H2AX. *Mutat Res.* 2012; 741: 57–64.
- 24 Ha L, Ceryak S, Patierno SR. Generation of S phase-dependent DNA double-strand breaks by Cr (VI) exposure: involvement of ATM in Cr (VI) induction of gamma-H2AX. *Carcinogenesis.* 2004; 25: 2265–74.
- 25 Albino AP, Jorgensen ED, Rainey P, Gillman G, Clark TJ, Gietl D, et al. gammaH2AX: A potential DNA damage response biomarker for assessing toxicological risk of tobacco products. *Mutat Res.* 2009; 678: 43–52.
- 26 Pacurari M, Yin XJ, Zhao J, Ding M, Leonard SS, Schwegler-Berry D, et al. Raw single-wall carbon nanotubes induce oxidative stress and activate MAPKs, AP-1, NF-kappaB, and Akt in normal and malignant human mesothelial cells. *Environ Health Perspect.* 2008; 116: 1211–7.
- 27 Ahamed M, Karns M, Goodson M, Rowe J, Hussain SM, Schlager JJ, et al. DNA damage response to different surface chemistry of silver nanoparticles in mammalian cells. *Toxicol Appl Pharmacol.* 2008; 233: 404–10.
- 28 Trouiller B, Reliene R, Westbrook A, Solaimani P, Schiestl RH. Titanium dioxide nanoparticles induce DNA damage and genetic instability in vivo in mice. *Cancer Res.* 2009; 69: 8784–9.
- 29 Tsaousi A, Jones E, Case CP. The in vitro genotoxicity of orthopaedic ceramic (Al₂O₃) and metal (CoCr alloy) particles. *Mutat Res.* 2010; 697: 1–9.
- 30 Sergeant JA, Paget V, Chevillard S. Toxicity and genotoxicity of nano-SiO₂ on human epithelial intestinal HT-29 cell line. *Ann Occup Hyg.* 2012; 56: 622–30.
- 31 Wan R, Mo Y, Feng L, Chien S, Tollerud DJ, Zhang Q. DNA damage caused by metal nanoparticles: involvement of oxidative stress and activation of ATM. *Chem Res Toxicol.* 2012; 25: 1402–11.
- 32 Toduka Y, Toyooka T, Ibuki Y. Flow cytometric evaluation of nanoparticles using side-scattered light and reactive oxygen species-mediated fluorescence-correlation with genotoxicity. *Environ Sci Technol.* 2012; 46: 7629–36.
- 33 Ozaki T, Nagase T, Ichimiya S, Seki N, Ohiri M, Nomura N, et al. NFB1/KIAA0170 is a novel nuclear transcriptional transactivator with BRCT domain. *DNA Cell Biol.* 2000; 19: 475–85.
- 34 de Jager M, van Noort J, van Gent DC, Dekker C, Kanaar R, Wyman C. Human Rad50/Mre11 is a flexible complex that can tether DNA ends. *Mol Cell.* 2001; 8: 1129–35.
- 35 You Z, Chahwan C, Bailis J, Hunter T, Russell P. ATM activation and its recruitment to damaged DNA require binding to the C terminus of Nbs1. *Mol Cell Biol.* 2005; 25: 5363–79.
- 36 Falck J, Coates J, Jackson SP. Conserved modes of recruitment of ATM, ATR and DNA-PKcs to sites of DNA damage. *Nature.* 2005; 434: 605–11.
- 37 Burma S, Chen BP, Murphy M, Kurimasa A, Chen DJ. ATM phosphorylates histone H2AX in response to DNA double-strand breaks. *J Biol Chem.* 2001; 276: 42462–7.
- 38 Stiff T, O'Driscoll M, Rief N, Iwabuchi K, Lobrich M, Jeggo PA. ATM and DNA-PK function redundantly to phosphorylate H2AX after exposure to ionizing radiation. *Cancer Res.* 2004; 64: 2390–6.
- 39 Stucki M, Clapperton JA, Mohammad D, Yaffe MB, Smerdon SJ, Jackson SP. MDC1 directly binds phosphorylated histone H2AX to regulate cellular responses to DNA double-strand breaks. *Cell.* 2005; 123: 1213–26.
- 40 Lou Z, Minter-Dykhouse K, Franco S, Gostissa M, Rivera MA, Celeste A, et al. MDC1 maintains genomic stability by participating in the amplification of ATM-dependent DNA damage signals. *Mol Cell.* 2006; 21: 187–200.
- 41 Wang J, Gong Z, Chen J. MDC1 collaborates with TopBP1 in DNA replication checkpoint control. *J Cell Biol.* 2011; 193: 267–73.
- 42 Shang YL, Boder AJ, Chen PL. NFB1, a novel nuclear protein with signature motifs of FHA and BRCT, and an internal 41-amino acid repeat sequence, is an early participant in DNA damage response. *J Biol Chem.* 2003; 278: 6323–9.
- 43 So S, Davis AJ, Chen DJ. Autophosphorylation at serine 1981 stabilizes ATM at DNA damage sites. *J Cell Biol.* 2009; 187: 977–90.
- 44 Lou Z, Minter-Dykhouse K, Wu X, Chen J. MDC1 is coupled to activated CHK2 in mammalian DNA damage response pathways. *Nature.* 2003; 421: 957–61.
- 45 Zhang J, Ma Z, Treszezamsky A, Powell SN. MDC1 interacts with Rad51 and facilitates homologous recombination. *Nat Struct Mol Biol.* 2005; 12: 902–9.

- 46 Wu L, Luo K, Lou Z, Chen J. MDC1 regulates intra-S-phase checkpoint by targeting NBS1 to DNA double-strand breaks. *Proc Natl Acad Sci USA*. 2008; 105: 11200–5.
- 47 Spycher C, Miller ES, Townsend K, Pavic L, Morrice NA, Janscak P, et al. Constitutive phosphorylation of MDC1 physically links the MRE11-RAD50-NBS1 complex to damaged chromatin. *J Cell Biol*. 2008; 181: 227–40.
- 48 Melander F, Bekker-Jensen S, Falck J, Bartek J, Mailand, N, Lukas, J. Phosphorylation of SDT repeats in the MDC1 N terminus triggers retention of NBS1 at the DNA damage-modified chromatin. *J Cell Biol*. 2008; 181: 213–26.
- 49 Chapman JR, Jackson SP. Phospho-dependent interactions between NBS1 and MDC1 mediate chromatin retention of the MRN complex at sites of DNA damage. *EMBO Rep*. 2008; 9: 795–801.
- 50 Mailand N, Bekker-Jensen S, Fastrup H, Melander F, Bartek J, Lukas C, et al. RNF8 ubiquitylates histones at DNA double-strand breaks and promotes assembly of repair proteins. *Cell*. 2007; 131: 887–900.
- 51 Huen MS, Grant R, Manke I, Minn K, Yu X, Yaffe MB, et al. RNF8 transduces the DNA-damage signal via histone ubiquitylation and checkpoint protein assembly. *Cell*. 2007; 131: 901–14.
- 52 Kolas NK, Chapman JR, Nakada S, Ylanko J, Chahwan R, Sweeney FD, et al. Orchestration of the DNA-damage response by the RNF8 ubiquitin ligase. *Science*. 2007; 318: 1637–40.
- 53 Lou Z, Chen BP, Asaithamby A, Minter-Dykhouse K, Chen DJ, Chen J. MDC1 regulates DNA-PK autophosphorylation in response to DNA damage. *J Biol Chem*. 2004; 279: 46359–62.
- 54 Nakanishi M, Ozaki T, Yamamoto H, Hanamoto T, Kikuchi H, Furuya K, et al. NFB1/MDC1 associates with p53 and regulates its function at the crossroad between cell survival and death in response to DNA damage. *J Biol Chem*. 2007; 282: 22993–3004.
- 55 Eliezer Y, Argaman L, Rhie A, Doherty AJ, Goldberg M. The direct interaction between 53BP1 and MDC1 is required for the recruitment of 53BP1 to sites of damage. *J Biol Chem*. 2009; 284: 426–35.
- 56 Coster G, Hayouka Z, Argaman L, Strauss C, Friedler A, Brandeis M, et al. The DNA damage response mediator MDC1 directly interacts with the anaphase-promoting complex/cyclosome. *J Biol Chem*. 2007; 282: 32053–64.
- 57 Inoue K, Nakanishi M, Kikuchi H, Yamamoto H, Todo S, Nakagawara A, et al. NFB1/MDC1 stabilizes oncogenic MDM2 to contribute to cell fate determination in response to DNA damage. *Biochem Biophys Res Commun*. 2008; 371: 829–33.
- 58 Luo K, Yuan J, Chen J, Lou Z. Topoisomerase II α controls the decatenation checkpoint. *Nat Cell Biol*. 2009; 11: 204–10.
- 59 Ihaka R, Gentleman R. R: A language for data analysis and graphics. *Journal of computational and graphical statistics*. 1996; 3: 299–314.
- 60 Pau G, Fuchs F, Sklyar O, Boutros M, Huber W. E-Blmage—an R package for image processing with applications to cellular phenotypes. *Bioinformatics*. 2010; 26: 979–81.
- 61 Strumberg D, Pilon AA, Smith M, Hickey R, Malkas L, Pommier Y. Conversion of topoisomerase I cleavage complexes on the leading strand of ribosomal DNA into 5'-phosphorylated DNA double-strand breaks by replication runoff. *Mol Cell Biol*. 2000; 20: 3977–87.
- 62 Andoh T, Ide T. Strand scission and rejoining of DNA in cultured mammalian cells induced by 4-nitroquinoline 1-oxide. *Cancer Res*. 1972; 32: 1230–5.
- 63 Frankenberg-Schwager M, Kirchermeier D, Greif G, Baer K, Becker M, Frankenberg D. Cisplatin-mediated DNA double-strand breaks in replicating but not in quiescent cells of the yeast *Saccharomyces cerevisiae*. *Toxicology*. 2005; 212: 175–84.
- 64 Celotti L, Ferraro P, Furlan D, Zanesi N, Pavanello S. DNA repair in human lymphocytes treated in vitro with (+)-anti- and (+/-)-syn-benzo[a]pyrene diolepoxide. *Mutat Res*. 1993; 294: 117–26.
- 65 Hsiang YH, Hertzberg R, Hecht S, Liu LF. Camptothecin induces protein-linked DNA breaks via mammalian DNA topoisomerase I. *J Biol Chem*. 1985; 260: 14873–8.
- 66 Bendixen C, Thomsen B, Alsner J, Westergaard O. Camptothecin-stabilized topoisomerase I-DNA adducts cause premature termination of transcription. *Biochemistry*. 1990; 29: 5613–9.
- 67 Sordet O, Redon CE, Guirouilh-Barbat J, Smith S, Solier S, Douarre C, et al. Ataxia telangiectasia mutated activation by transcription- and topoisomerase I-induced DNA double-strand breaks. *EMBO Rep*. 2009; 10: 887–93.
- 68 Minca EC, Kowalski D. Replication fork stalling by bulky DNA damage: localization at active origins and checkpoint modulation. *Nucleic Acids Res*. 2011; 39: 2610–23.
- 69 Jones CJ, Edwards SM, Waters R. The repair of identified large DNA adducts induced by 4-nitroquinoline-1-oxide in normal or xeroderma pigmentosum group A human fibroblasts, and the role of DNA polymerases α or δ . *Carcinogenesis*. 1989; 10: 1197–201.
- 70 Pulkrabek P, Leffler S, Grunberger D, Weinstein IB. Modification of deoxyribonucleic acid by a diol epoxide of benzo[a]pyrene. Relation to deoxyribonucleic acid structure and conformation and effects on transcriptional activity. *Biochemistry*. 1979; 18: 5128–34.
- 71 Cleaver JE. Defective repair replication of DNA in xeroderma pigmentosum. *Nature*. 1968; 218: 652–6.
- 72 Setlow RB, Regan JD, German J, Carrier WL. Evidence that xeroderma pigmentosum cells do not perform the first step in the repair of ultraviolet damage to their DNA. *Proc Natl Acad Sci USA*. 1969; 64: 1035–41.
- 73 Volker M, Mone MJ, Karmakar P, van Hoffen A, Schul W, Vermeulen W, et al. Sequential assembly of the nucleotide excision repair factors in vivo. *Mol Cell*. 2001; 8: 213–24.
- 74 Matsumoto M, Yaginuma K, Igarashi A, Imura M, Hasegawa M, Iwabuchi K, et al. Perturbed gap-filling synthesis in nucleotide excision repair causes histone H2AX phosphorylation in human quiescent cells. *J Cell*

- Sci. 2007; 120: 1104–12.
- 75 Hanasoge S, Ljungman M. H2AX phosphorylation after UV irradiation is triggered by DNA repair intermediates and is mediated by the ATR kinase. *Carcinogenesis*. 2007; 28: 2298–304.
- 76 Vu VT, Grantham PH, Roller PP, Hankins WD, Wirth PJ, Thorgeirsson SS. Formation of DNA adducts from N-acetoxy-2-acetylaminofluorene and N-hydroxy-2-acetylaminofluorene in rat hemopoietic tissues in vivo. *Cancer Res*. 1986; 46: 233–8.
- 77 Marti TM, Hefner E, Feeney L, Natale V, Cleaver JE. H2AX phosphorylation within the G1 phase after UV irradiation depends on nucleotide excision repair and not DNA double-strand breaks. *Proc Natl Acad Sci USA*. 2006; 103: 9891–6.
- 78 Matsuda T, Yagi T, Takebe H, Matsui S. Detection and quantification of DNA strand breaks in human cells induced by contaminants in Japanese tap waters. *Water Science and Technology*. 1996; 33: 297–304.
- 79 Pegg AE. Methylation of the O6 position of guanine in DNA is the most likely initiating event in carcinogenesis by methylating agents. *Cancer Invest*. 1984; 2: 223–31.
- 80 Zak P, Kleibl K, Laval F. Repair of O6-methylguanine and O4-methylthymine by the human and rat O6-methylguanine-DNA methyltransferases. *J Biol Chem*. 1994; 269: 730–3.
- 81 Oh HK, Teo AK, Ali RB, Lim A, Ayi TC, Yarosh DB, et al. Conformational change in human DNA repair enzyme O6-methylguanine-DNA methyltransferase upon alkylation of its active site by SN1 (indirect-acting) and SN2 (direct-acting) alkylating agents: breaking a “salt-link”. *Biochemistry*. 1996; 35: 12259–66.
- 82 Dolan ME, Moschel RC, Pegg AE. Depletion of mammalian O6-alkylguanine-DNA alkyltransferase activity by O6-benzylguanine provides a means to evaluate the role of this protein in protection against carcinogenic and therapeutic alkylating agents. *Proc Natl Acad Sci USA*. 1990; 87: 5368–72.
- 83 Pegg AE, Boosalis M, Samson L, Moschel RC, Byers TL, Swenn K, et al. Mechanism of inactivation of human O6-alkylguanine-DNA alkyltransferase by O6-benzylguanine. *Biochemistry*. 1993; 32: 11998–2006.
- 84 Ceccotti S, Aquilina G, Macpherson P, Yamada M, Karan P, Bignami M. Processing of O6-methylguanine by mismatch correction in human cell extracts. *Curr Biol*. 1996; 6: 1528–31.
- 85 Duckett DR, Drummond JT, Murchie AI, Reardon JT, Sancar A, Lilley DM, et al. Human MutSalpha recognizes damaged DNA base pairs containing O6-methylguanine, O4-methylthymine, or the cisplatin-d (GpG) adduct. *Proc Natl Acad Sci USA*. 1996; 93: 6443–7.
- 86 Grilley M, Griffith J, Modrich P. Bidirectional excision in methyl-directed mismatch repair. *J Biol Chem*. 1993; 268: 11830–7.
- 87 Shimizu Y, Nakatsuru Y, Ichinose M, Takahashi Y, Kume H, Mimura J, et al. Benzo[a]pyrene carcinogenicity is lost in mice lacking the aryl hydrocarbon receptor. *Proc Natl Acad Sci USA*. 2000; 97: 779–82.
- 88 Harper PA, Prokipcak RD, Bush LE, Golas CL, Okey AB. Detection and characterization of the Ah receptor for 2,3,7,8-tetrachlorodibenzo-p-dioxin in the human colon adenocarcinoma cell line LS180. *Arch Biochem Biophys*. 1991; 290: 27–36.
- 89 Nebert DW, Roe AL, Dieter MZ, Solis WA, Yang Y, Dalton TP. Role of the aromatic hydrocarbon receptor and [Ah] gene battery in the oxidative stress response, cell cycle control, and apoptosis. *Biochem Pharmacol*. 2000; 59: 65–85.
- 90 Gelboin HV. Benzo[alpha]pyrene metabolism, activation and carcinogenesis: role and regulation of mixed-function oxidases and related enzymes. *Physiol Rev*. 1980; 60: 1107–66.
- 91 de Feraudy S, Revet I, Bezrookove V, Feeney L, Cleaver JE. A minority of foci or pan-nuclear apoptotic staining of gammaH2AX in the S phase after UV damage contain DNA double-strand breaks. *Proc Natl Acad Sci USA*. 2010; 107: 6870–5.
- 92 Meyer B, Voss KO, Tobias F, Jakob B, Durante M, Taucher-Scholz G. Clustered DNA damage induces pan-nuclear H2AX phosphorylation mediated by ATM and DNA-PK. *Nucleic Acids Res*. 2013; 41: 6109–18.